

## Interpolation of vector fields from human cardiac DT-MRI

This article has been downloaded from IOPscience. Please scroll down to see the full text article.

2011 Phys. Med. Biol. 56 1415

(<http://iopscience.iop.org/0031-9155/56/5/013>)

View [the table of contents for this issue](#), or go to the [journal homepage](#) for more

Download details:

IP Address: 195.220.108.241

The article was downloaded on 21/02/2011 at 15:43

Please note that [terms and conditions apply](#).

# Interpolation of vector fields from human cardiac DT-MRI

F Yang<sup>1</sup>, Y M Zhu<sup>1</sup>, S Rapacchi<sup>1</sup>, J H Luo<sup>2</sup>, M Robini<sup>1</sup> and P Croisille<sup>1</sup>

<sup>1</sup> CREATIS, CNRS UMR 5220, Inserm U630, INSA Lyon, University of Lyon 1, University of Lyon, Villeurbanne, France

<sup>2</sup> College of Life Science and Technology, Shanghai Jiaotong University, 200240, Shanghai, People's Republic of China

E-mail: [feng.yang@creatis.insa-lyon.fr](mailto:feng.yang@creatis.insa-lyon.fr)

Received 2 July 2010, in final form 9 November 2010

Published 11 February 2011

Online at [stacks.iop.org/PMB/56/1415](http://stacks.iop.org/PMB/56/1415)

## Abstract

There has recently been increased interest in developing tensor data processing methods for the new medical imaging modality referred to as diffusion tensor magnetic resonance imaging (DT-MRI). This paper proposes a method for interpolating the primary vector fields from human cardiac DT-MRI, with the particularity of achieving interpolation and denoising simultaneously. The method consists of localizing the noise-corrupted vectors using the local statistical properties of vector fields, removing the noise-corrupted vectors and reconstructing them by using the thin plate spline (TPS) model, and finally applying global TPS interpolation to increase the resolution in the spatial domain. Experiments on 17 human hearts show that the proposed method allows us to obtain higher resolution while reducing noise, preserving details and improving direction coherence (DC) of vector fields as well as fiber tracking. Moreover, the proposed method perfectly reconstructs azimuth and elevation angle maps.

(Some figures in this article are in colour only in the electronic version)

## 1. Introduction

Diffusion tensor magnetic resonance imaging (DT-MRI, or DTI) is a new technique allowing *ex vivo* and *in vivo* investigation of the structural properties of fibrous tissues by measuring the relative diffusion of water molecules in different directions (Basser *et al* 1994a, Basser *et al* 1994b). In DT-MRI, to analyze the fiber architecture of brain white matter or of the myocardium, fiber tracking or tractography is often performed from the primary eigenvectors of diffusion tensors. However, due to technical limitations of MRI machines, DT-MRI is sensitive to the difficult compromise between spatial resolution and noise or artifacts (Basser

and Pajevic 2000). This is particularly true for cardiac DT-MRI. Consequently, computed primary vector fields are often subject to noise or artifacts, which results in harmful impacts on the quality of fiber tracking. Hence, the denoising of vector fields in DT-MRI is an important means for relaxation of acquisition constraints as well as for applications such as fiber tracking. Meanwhile, in the case of human cardiac DT-MRI, the acquired data are rather sparse in some parts of the myocardium because of the low spatial resolution, and the myocardium appears discontinuous. In order to better describe the myocardium, it is necessary to perform data interpolation which can be performed at the level of diffusion-weighted (DW) images, or at the level of tensor fields or vector fields. However, in some situations, the only available information is a vector field. This is the case when we track fibers from vector fields using the most common streamline fiber tracking algorithm that is directly based on primary vector fields, or when we have no possibility of coming back to tensor fields or DW images, or still when it is not necessary to come back to tensor fields or DW images. For example, when tracking fibers from polarized light microscopy data, the only information available is the elevation angle map and the azimuth angle map (Jouk *et al* 2000), which allow calculating primary vector fields but are not sufficient to reconstruct tensor fields or DW images.

To denoise vector fields, the most popular vector filter is the vector median filter (Astola *et al* 1990), which is widely used to remove impulse noise. To improve its performance in the case of additive Gaussian noise, vector median filtering can be combined with linear filtering (Astola *et al* 1990) or extended to the weighted vector median filtering (Viero *et al* 1994). Other general purpose vector filters include vector directional filters that eliminate atypical directions (Trahanias *et al* 1996), partial differential equation-based (PDE-based) regularization methods (Tschumperlé and Deriche 2003), and wavelet-based denoising techniques (Xia and Suter 1996, Westenberg and Ertl 2004, 2005). In the case of vector fields computed from DT-MRI data, Yoruk and Acar (2005) have proposed a PDE-based method to regularize primary diffusion vector fields, which is based on a structure-sensitive function derived from local orientation similarity. A variational approach to restoring primary eigenvector fields has been addressed by Coulon *et al* (2004); the task is to minimize a total-variation-based energy defined for the direction map. Cathier and Ayache (2004) have proposed a vector field regularization method focused on the non-rigid registration by combining the vector convolution filter and vectorial spline, which are deduced from isotropic differential quadratic forms of two-dimensional (2D) deformation vector fields.

Meanwhile, the interpolation of vector fields to improve fiber tracking from DT-MRI data is also addressed in the literature. Zhao *et al* (2005) have proposed to interpolate primary vector components weighted by fractional anisotropy (FA). Kim *et al* (2004) have introduced a selective eigenvector interpolation method which uses a thresholded inner product to determine the weights associated with the eigenvectors. These methods however present drawbacks, since the vector components in practical applications are generally correlated. This correlation is not accounted for, if vector components are processed independently. In fact, interpolating noisy vector fields can introduce erroneous vectors and do not facilitate fiber tracking at all. This led us to investigate a method that allows interpolating vector fields while denoising. A preliminary work based on this idea is reported in Yang *et al* (2009). Our noise-reduced interpolation method removes the noise-corrupted vectors rather than denoising the whole vector field in a uniform manner, and uses the thin plate spline (TPS) model (Duchon 1977, Bookstein 1989, Sprengel *et al* 1996, Davis *et al* 1997) in order to exploit the correlation between vector components for vector field interpolation with desirable properties. More precisely, the method first localizes and removes the noise-corrupted vectors using a vector-homogeneity criterion, and then restores the noise-corrupted vectors using local TPS interpolation. Then global TPS interpolation of the denoised vector field is performed

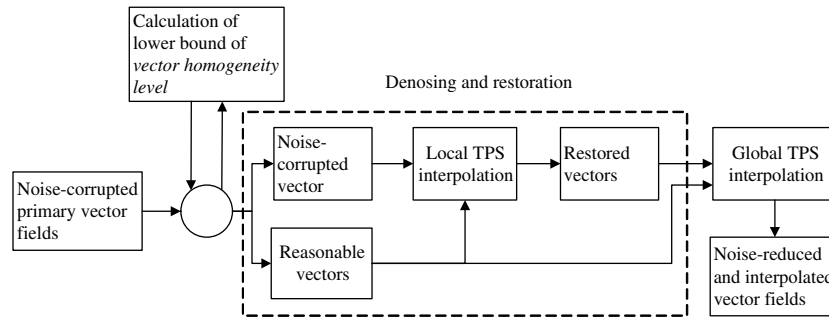


**Figure 1.** Flowchart of the proposed noise-reduced interpolation of the primary vector fields. The input is a noise-corrupted vector field, and the output is a denoised and interpolated vector field. The dotted rectangle indicates the block of noise-corrupted vector denoising and restoration.

to increase spatial resolution. The paper is organized as follows: the proposed method is described in section 2, experiments and results are given in section 3, and sections 4 and 5 discuss the results and conclude the study, respectively.

## 2. Noise-reduced interpolation scheme

The proposed noise-reduced interpolation is decomposed into three steps: localization of noise-corrupted vectors, local restoration of these erroneous vectors, and global interpolation of the whole vector field. The first step aims at determining the presence of noise-corrupted vectors in a chosen window according to the vector-homogeneity level. The second aims to restore the noise-corrupted vectors by local TPS interpolation and the third to interpolate the whole primary vector field to obtain higher spatial resolution. The flowchart of such noised-reduced interpolation for the primary vector fields using TPS interpolation is shown in figure 1.

### 2.1. Localization of noise-corrupted vectors

Since eigenvector fields in DT-MRI are not directly produced by MRI machines, but calculated from tensor fields that in turn are derived from raw DW images, the influence of noise on eigenvector fields is difficult to apprehend. We can nevertheless say that if DW images are noisy, the subsequently obtained eigenvector fields will be more or less noisy. A straightforward denoising method would be to simply denoise the whole vector field, which may introduce over smoothing. The idea here is to perform denoising only where it is necessary. To do that, we define the so-called noise-corrupted vectors. Since vectors from any physical DT-MRI always present some spatial correlation, the direction of a vector should not deviate arbitrarily from the directions of its neighboring vectors (Holmes *et al* 2000). This leads us to introduce the notion of the vector-homogeneity level to measure the correlation between neighboring vectors. Given a vector field associated with a data slice, we slide a  $Q \times Q$  window in a non-overlapping way, from left to right and from top to bottom. Inside a given window, all the vectors in the current window are involved in the calculation of the vector-homogeneity level, and each of them is considered in turn as the current vector, whose vector-homogeneity level is computed by comparing it with the other vectors inside the window. Let  $\mathbf{v}(x_0, y_0, z_0)$  denote the current vector and let  $\{\mathbf{v}(x_k, y_k, z_k)\}_{k=1}^{Q^2-1}$  be its

neighboring vectors inside the current window. The vector-homogeneity level of  $\mathbf{v}(x_0, y_0, z_0)$  is defined by

$$d(x_0, y_0, z_0) = \frac{1}{Q^2 - 1} \sum_{k=1}^{Q^2-1} (\mathbf{v}(x_0, y_0, z_0) \cdot \mathbf{v}(x_k, y_k, z_k)). \quad (1)$$

Note that, if the window size is too small, say  $2 \times 2$ , the neighborhood information is not sufficient to measure the correlation between neighboring vectors. In contrast, if the window size is too large, say  $8 \times 8$ , too many neighboring vectors are involved and normal vectors may be erroneously confused as noise-corrupted vectors. We found from our experiments that a size of  $4 \times 4$  gives the best results in terms of localization of noise-corrupted vectors.

When the eigenvectors are of unit length, the inner product  $\mathbf{v}(x_0, y_0, z_0) \cdot \mathbf{v}(x_k, y_k, z_k)$  reflects the cosine angle value between  $\mathbf{v}(x_0, y_0, z_0)$  and  $\mathbf{v}(x_k, y_k, z_k)$ , and the vector-homogeneity level  $d(x_0, y_0, z_0)$  will be the mean of the cosines of angles between  $\mathbf{v}(x_0, y_0, z_0)$  and its  $Q^2-1$  neighbors and will have a value between  $-1$  and  $1$ , as the angle between two vectors is  $[0, \pi]$ .

We determine the noise-corrupted vectors by fixing a low bound of the vector-homogeneity level. If  $d(x_0, y_0, z_0)$  is smaller than this bound, the vector  $\mathbf{v}(x_0, y_0, z_0)$  is considered to be incoherent with respect to its neighboring vectors and is regarded as a noise-corrupted vector. In this sense, the vectors, whose directions are incoherent with those of their neighbors due to the ambiguity between  $+\mathbf{v}$  and  $-\mathbf{v}$  when calculating eigenvectors from diffusion tensors, will be considered as noise-corrupted vectors and therefore will be discarded and restored in the next step. Such localization of noise-corrupted vectors avoids introducing unnecessary smoothing of the vector field to be interpolated.

## 2.2. Restoration of noise-corrupted vectors

Once the noise-corrupted vectors are localized, they are first discarded and then restored by interpolating their neighbors. To do this, we use the TPS interpolation for its ability of accounting for the correlation among vector components and for its smoothing property (Duchon 1977, Bookstein 1989).

The name ‘thin plate spline’ refers to a physical analogy involving the bending of a thin sheet of metal. TPS was initially proposed for image registration to obtain the coordinates in the deformed image from a limited set of control points in the original image together with their positions in the deformed image (Duchon 1977, Bookstein 1989, Sprengel *et al* 1996, Davis *et al* 1997). Our immediate purpose here is to restore the noise-corrupted vectors, but TPS interpolation will also be used to increase the spatial resolution of the vector fields specified by irregular points and corresponding vectors, as described in the next subsection.

Three dimensional (3D) TPS interpolation can be described as follows:

$$\mathbf{f}(x, y, z) = \mathbf{a}_1 + \mathbf{a}_x x + \mathbf{a}_y y + \mathbf{a}_z z + \sum_{i=1}^n \mathbf{w}_i U |P_i - (x, y, z)|, \quad (2)$$

where  $\mathbf{f}(x, y, z)$  designates the vector at coordinate  $(x, y, z)$ ,  $P_i$  stands for the coordinates of control points and  $\mathbf{a}_1, \mathbf{a}_x, \mathbf{a}_y, \mathbf{a}_z \in \mathbb{R}^3$  in the first four terms are the global affine transform coefficients, while  $\mathbf{w}_i \in \mathbb{R}^3$  in the remaining terms are the local nonlinear transformation coefficients. The radial basis function  $U(r) = |r| = (x^2 + y^2 + z^2)^{1/2}$  is the fundamental solution of the biharmonic equation; it guarantees that the TPS function minimizes the bending

energies:

$$I(f) = \iiint_{R^3} (f_{xx}^2 + f_{yy}^2 + f_{zz}^2 + 2f_{xy}^2 + 2f_{xz}^2 + 2f_{yz}^2) dx dy dz, \quad (3)$$

where  $I(f)$  denotes the energy corresponding to one component of function  $\mathbf{f}(x, y, z)$ ,  $f_{xx}$ ,  $f_{yy}$ ,  $f_{zz}$  designate the second-order partial derivatives of  $f$ , and  $f_{xy}$ ,  $f_{xz}$ ,  $f_{yz}$  the second-order mixed derivatives of function  $f$ . Minimizing the bending energy ensures that the vector fields are optimally smooth (Bookstein 1989). For this property, we adopt TPS interpolation to restore the noise-corrupted vectors.

In a  $Q \times Q$  window, if a vector is identified as noise corrupted, other vectors inside this window will be taken as the landmarks for the TPS model to restore the noise-corrupted vector. To get better denoising results, the influence of noise-corrupted vectors in the neighborhood should be reduced as much as possible. To this end, when we choose the landmarks for restoration, we first determine whether the vector-homogeneity level of each neighboring vector is higher than some given low bound. If it is, this neighboring vector will be chosen as a landmark for TPS interpolation. Otherwise, it is discarded from the current restoration process. If the number of noise-corrupted vectors inside the current window is greater than one-third of the total number of vectors in the window, the neighborhood is considered as a region without clear majority. In this case, we do not denoise any vector in the window.

### 2.3. Global TPS interpolation of primary vector fields

After obtaining the noise-reduced vector field, we perform global TPS interpolation to obtain higher spatial resolution as well as more information for fiber tracking. For this purpose, we use only the vectors inside the myocardium as landmarks for the global TPS model so that the resulting interpolation of primary vector fields follows the whole TPS model conditioned by these landmarks. Vectors outside the myocardium are discarded by masks computed from the T2 images.

## 3. Experiments and results

### 3.1. Data acquisition

In our experiments, the primary vector fields were calculated from cardiac DT-MRI data corresponding to 17 human hearts. Most datasets were acquired under clinical conditions. They concern the cardiac diffusion-weighted (DW) images and T2 images, which were acquired from 16 *ex vivo* human hearts on Siemens 1.5 T Magnetom Sonata in the Neuro-Cardiology Hospital of Lyon with the following settings: TE = 98 ms, TR = 8600 ms, FOV =  $256 \times 256$  mm<sup>2</sup>, slice thickness = 2 mm, slice spacing = 2 mm, number of slices = 52, slice size =  $128 \times 128$ , diffusion sensitivity  $b = 1000$  s mm<sup>-2</sup>, gradient directions = 30 or 12 or 6. The sequence used was a 2D EPI diffusion-weighted sequence with a twice-refocused diffusion preparation. The acquisition time for a 3D dataset with 30 directions and 1 average was about 5 min. Each heart was located in a plastic container and fixed by a hydrophilic gel to maintain a diastolic shape. This setup has a low dielectric effect and also eliminates unwanted susceptibility artifacts near the boundaries of the heart. The primary vector fields to be interpolated were calculated from these DW images and T2 images.

One cardiac DT-MRI dataset serves as a reference. It was acquired using repeated accumulation over a very long time (more than 48 h) to obtain a very high signal-to-noise ratio. This dataset, which was in the form of vector fields, was downloaded from the web site <http://www.ccbm.jhu.edu/research/DTMRIDS.php>. The corresponding acquisition

parameters are the following: gradient directions = 19, resolution =  $0.4297 \times 0.4297 \times 1.0 \text{ mm}^3$ , size =  $256 \times 256 \times 134$ . The primary eigenvector field of the dataset was undersampled by a factor of 4 (in each direction) and then corrupted by additive Gaussian noise. Since vector components are correlated with each other, it is not appropriate to add noise to each component independently. Instead, we added Gaussian noise to azimuth and elevation angles of the primary vector fields, which define the primary eigenvector's direction. The standard deviations of the added Gaussian noises range from 0.032 to 0.224. These standard deviation values seem to be small but they are in fact fairly high for vector field data as they are added to the normalized elevation azimuth angles. We define the noisy vector percentage (NVP) as the ratio of the standard deviation of the noise  $\sigma_N$  to that of the reference vector field  $\sigma_R$ :

$$\left\{ \begin{array}{l} \text{NVP} = \frac{\sigma_N}{\sigma_R} \times 100\% \\ \sigma_N = \left( \frac{1}{M \times N} \sum_{i=1}^M \sum_{j=1}^N (nx_{ij} - \bar{nx})^2 + (ny_{ij} - \bar{ny})^2 + (nz_{ij} - \bar{nz})^2 \right)^{\frac{1}{2}} \\ \sigma_R = \left( \frac{1}{M \times N} \sum_{i=1}^M \sum_{j=1}^N (x_{ij} - \bar{x})^2 + (y_{ij} - \bar{y})^2 + (z_{ij} - \bar{z})^2 \right)^{\frac{1}{2}} \end{array} \right. , \quad (4)$$

where  $(x_{ij}, y_{ij}, z_{ij})$  stands for the three vector components of a reference vector field,  $(nx_{ij}, ny_{ij}, nz_{ij})$  designates the vector component subtraction of the corresponding reference vector field from the noisy vector field,  $(\bar{x}, \bar{y}, \bar{z})$  and  $(\bar{nx}, \bar{ny}, \bar{nz})$ , respectively, indicate the mean reference vector and the mean noise vector, and  $M \times N$  is the size of the given slices. The NVP values corresponding to the Gaussian noise standard deviation values in [0.032, 0.224] on elevation and azimuth angles range from 13.73% to 80.42% in the primary vector fields. Note that a greater NVP value indicates a lower SNR or a noisier vector field.

### 3.2. Performance evaluation

The proposed noise-reduced interpolation method is assessed in terms of various criteria, in both qualitative and quantitative manners.

The downsampled and noisy reference vector fields are interpolated using the proposed method and bilinear interpolation, and the results are compared with the reference in terms of azimuth and elevation angle maps.

The elevation angle corresponds to the angle between the fiber and the section plane (shown as  $\varepsilon$  in figure 2), while the azimuth angle represents the angle between the projection of the fiber on the section plane and the east-west axis of the same plane (shown as  $\alpha$  in figure 2). The knowledge of these two angles which should range from 0 to  $\pi$  for the azimuth angle and from  $-\pi/2$  to  $\pi/2$  for the elevation angle completely determines the direction of the fiber.

The quality of the elevation and azimuth angle maps is assessed using criteria that concern the mean absolute error  $\text{ME} = (1/M \times N) \sum_{i=1}^M \sum_{j=1}^N |X(i, j) - X_0(i, j)|$ , the standard deviation  $\text{MSE} = ((1/M \times N) \sum_{i=1}^M \sum_{j=1}^N (|X(i, j) - X_0(i, j)| - \text{ME})^2)^{1/2}$  and the correlation coefficient  $r = \sum_{i=1}^M \sum_{j=1}^N (X(i, j) - \bar{X})(X_0(i, j) - \bar{X}_0) / (\sum_{i=1}^M \sum_{j=1}^N (X(i, j) - \bar{X})^2 (X_0(i, j) - \bar{X}_0)^2)^{\frac{1}{2}}$ , where  $X$  and  $X_0$  denote the interpolated and the reference images, and  $\bar{X}$  and  $\bar{X}_0$  stand for their respective means.

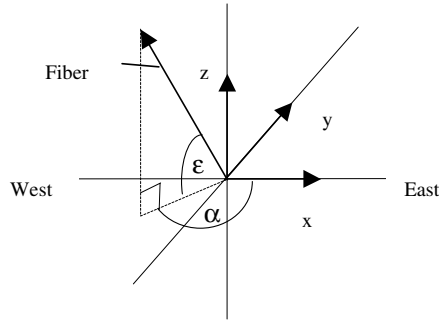


**Figure 2.** Azimuth angle  $\alpha$  and elevation angle  $\varepsilon$  of a fiber.

The performance of the proposed interpolation method is also assessed in terms of direction map, fiber tracking, and direction coherence (DC). The DC index we introduce here aims to evaluate the robustness of the denoising and describe the local vector coherence:

$$DC = 20 \lg(C_c/C_i) \quad (5)$$

where  $C_c$  and  $C_i$  denote the number of normal vectors and that of noise-corrupted vectors, respectively. A vector is considered as normal or noise corrupted depending on its vector-homogeneity level defined by equation (1). A greater  $C_c$  or a smaller  $C_i$  indicates more neighboring vectors having close directions and hence a greater DC value means more regular vector fields.

Finally, the influence of vector field interpolation on fiber architecture is assessed by comparing the fiber tracking results obtained from the DW images without interpolation, from the interpolated vector fields and from the interpolated tensor fields. In addition, to compare fiber tracking results from vector field interpolation and tensor field interpolation under the same conditions, we have extended the TPS interpolation to tensor fields as follows. As demonstrated in Arsigny *et al* (2005, 2006), tensor interpolation in Euclidean space can introduce a swelling effect. To avoid this problem, we take the logarithm of a diffusion tensor  $\mathbf{D} = [D_{xx}, D_{xy}, D_{xz}; D_{xy}, D_{yy}, D_{yz}; D_{xz}, D_{yz}, D_{zz}]$  using the method described in Arsigny *et al* (2006), then represent the logarithmically transformed tensor  $\mathbf{D}'$  by its six free components  $D'_{xx}, D'_{yy}, D'_{zz}, D'_{xy}, D'_{xz}, D'_{yz}$ , and finally apply the TPS model to the 6D vectors representing the logarithmically transformed diffusion tensors.

### 3.3. Results and discussions

Figure 3 shows the azimuth and elevation angle maps calculated from the primary vector fields obtained by using bilinear interpolation and the proposed noise-reduced interpolation. Figures 3(a) and (b) represent the original maps before undersampling and without adding noise. In figure 3(a), we can observe the continuous variation in a circular sense of azimuth angles inside the wall of the left ventricle, with the whole range of angles (colors) being visited twice. This variation in azimuth angles reflects the spiral-shaped muscle structure of the heart. A less clear succession of azimuth angles with the whole range of angles being visited only once is present in the right ventricular wall. In figure 3(b), we observe that the elevation angle varies from  $25^\circ$  in the endocardium to  $0^\circ$  in the midwall, and back to  $25^\circ$  in the epicardium for both the left ventricle (LV) and the right ventricle (RV), which reflects the fiber rotation.

The regular variation pattern of azimuth and elevation angle is preserved after both bilinear and our proposed interpolations. However, bilinear interpolation introduces many serrate artifacts around the contour of the ventricles in the elevation angle map, while

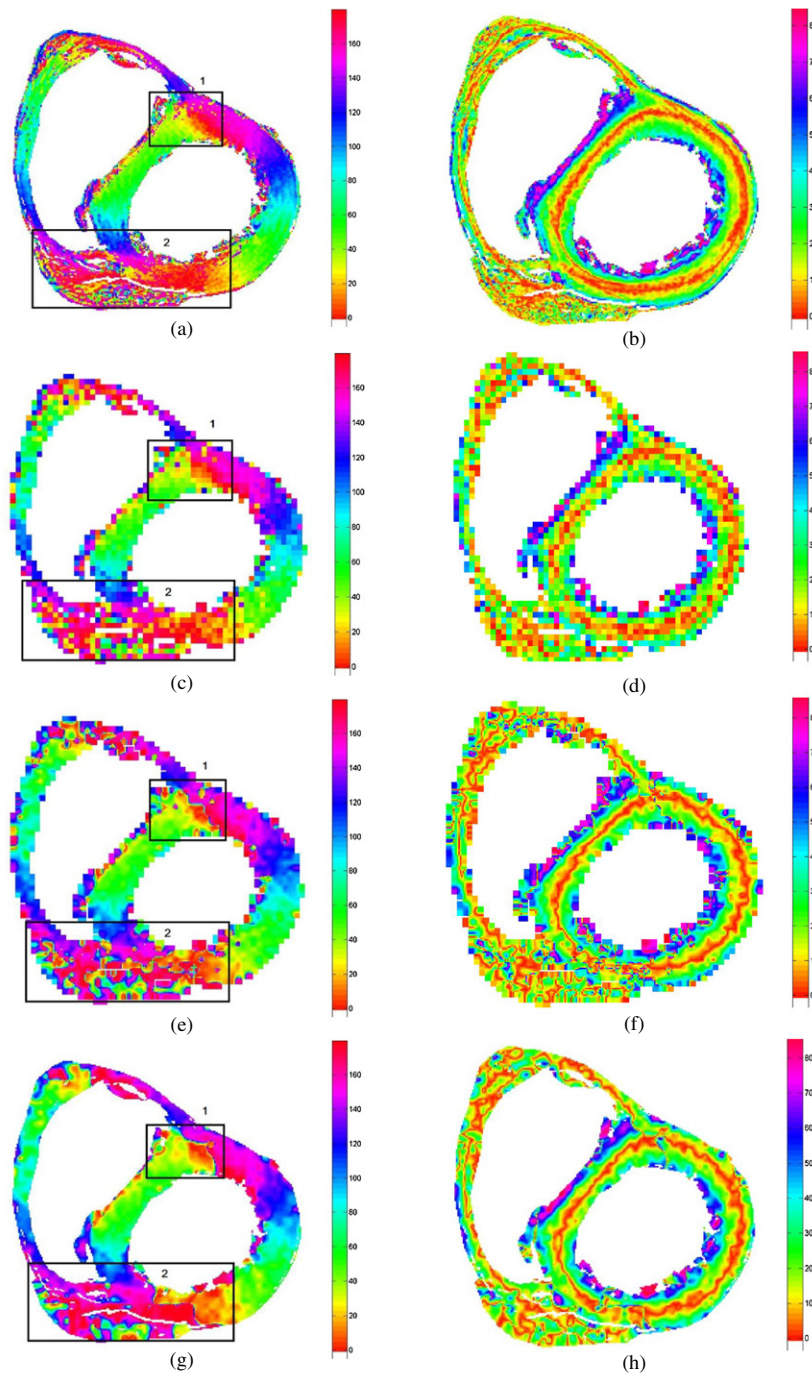


**Figure 3.** Azimuth angle maps (left column) and elevation angle maps (right column); (a) and (b) original angle maps before downsampling and without added noise; (c) and (d) angle maps after downsampling and addition of Gaussian noise (the percentage of noise-corrupted vectors is 13.73%); (e) and (f) angle maps calculated from the primary vector fields obtained by bilinear interpolation; (g) and (h) angle maps calculated from the primary vector fields obtained by using our noise-reduced interpolation.

**Table 1.** Quantitative analysis of angle maps obtained using bilinear interpolation and our noise-reduce interpolation for the same slice of a human heart.

NVP		13.73%		40.99%		80.42%	
		Bilinear	TPS	Bilinear	TPS	Bilinear	TPS
Elevation angle	Mean absolute error	5.307	2.845	6.565	3.993	9.4391	6.204
	Standard deviation	13.14	7.566	14.26	9.157	18.52	13.40
	Correlation coefficient	0.7589	0.9094	0.7313	0.8697	0.6557	0.7973
Azimuth angle	Mean absolute error	15.13	9.320	16.14	10.06	17.44	11.65
	Standard deviation	38.82	29.96	38.45	29.11	38.00	29.13
	Correlation coefficient	0.7342	0.8406	0.7330	0.8446	0.7264	0.8363

the elevation angle map obtained with the proposed method is very close to the reference (figure 3(b)). Similar results are observed for the azimuth angle. Bilinear interpolation produces serrate artifacts near the contour of the LV. In addition, (the rectangular) region 2, where the azimuth angle changes from  $120^\circ$  to  $180^\circ$  and then from  $0^\circ$  to  $20^\circ$ , becomes greatly confused after bilinear interpolation, and it is difficult to recognize the spiral-shaped succession of different azimuth angles in this region. Similar artifacts introduced by bilinear interpolation are visible in the regions having the same azimuth angle range in the right ventricle wall. By contrast, the azimuth angle map obtained with the proposed method is very smooth and close to the reference (figure 3(a)). The discontinuities of the azimuth angle observed in regions 1 and 2 with our method are due to the fact that the involved vectors (before interpolation) having opposite directions (azimuth angle varies from  $180^\circ$  to  $0^\circ$ ) are not noise-corrupted vectors and are interpolated directly.

Quantitative comparison results concerning the azimuth and elevation angle maps for the same slice of a heart obtained using bilinear interpolation and our method are summarized in table 1. Regardless of the NVP, our noise-reduced interpolation always yields significantly smaller mean absolute errors and standard deviations, and higher correlation coefficient than bilinear interpolation. In addition, the correlation coefficient with our method does not decrease significantly when the NVP increases. Especially for azimuth angles, the correlation coefficient even increases a little when the NVP increases from 13.73% to 40.99%, while the correlation coefficient with bilinear interpolation always decreases with the increase of NVP. This shows that our noise-reduced interpolation is more robust to noise. It is worth noting that the azimuth angle map exhibits much higher standard deviations than the elevation angle map regardless of the used interpolation method. This is because in some areas of the azimuth angle map (regions 1 and 2 in figure 3(a)), the direction of projections on the east-west axis of the corresponding fibers varies rapidly and abruptly so that a boundary between these rapidly changing vectors appears after interpolation using bilinear interpolation or our method. Moreover, if the vector field is very noisy (e.g. the right myocardium in region 2), it is impossible to interpolate it correctly using either bilinear interpolation (we can see it from the chaotic appearance in region 2) or the proposed method (although in this case the azimuth angle map in the same region is very smooth, it is still different from the azimuth angle map calculated from the reference vector field). As a consequence, the local direction of the fibers would become very disordered. For this situation, both interpolation methods produce artifacts in regions 1 and 2 which contribute to high standard deviation values for the azimuth angle map.

Figure 4 illustrates the results of noise-reduced interpolation for primary eigenvector fields corresponding to the tenth slice of a human heart dataset. The vector fields are

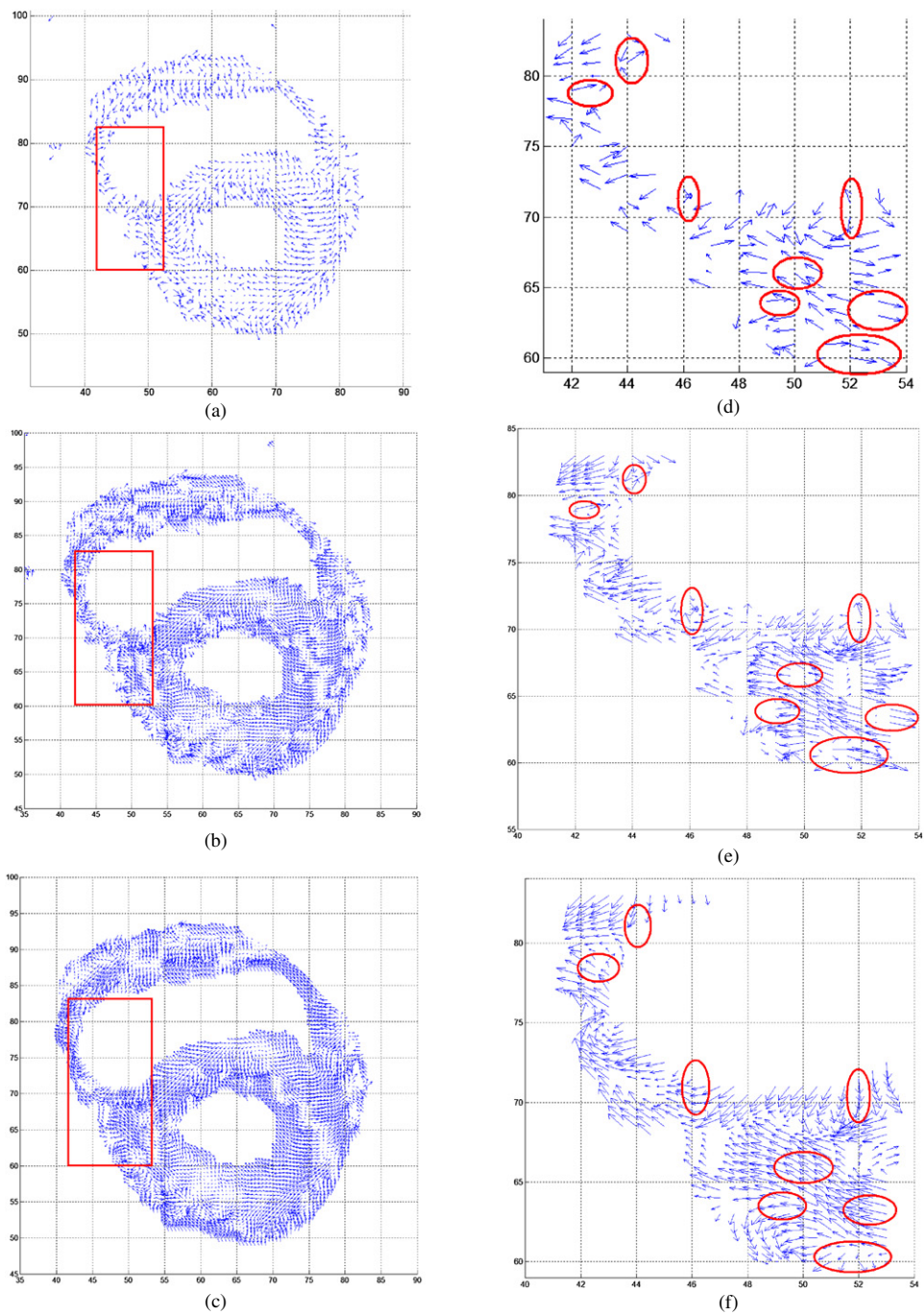


**Figure 4.** Results of noise-reduced interpolation of a primary eigenvector field corresponding to the tenth slice of a human heart dataset. (a) Original primary vector field. (b) Bilinear interpolation of the primary vector field. (c) Noise-reduced interpolation of the primary vector field. (d)–(f) The corresponding sparse regions marked with red rectangles.

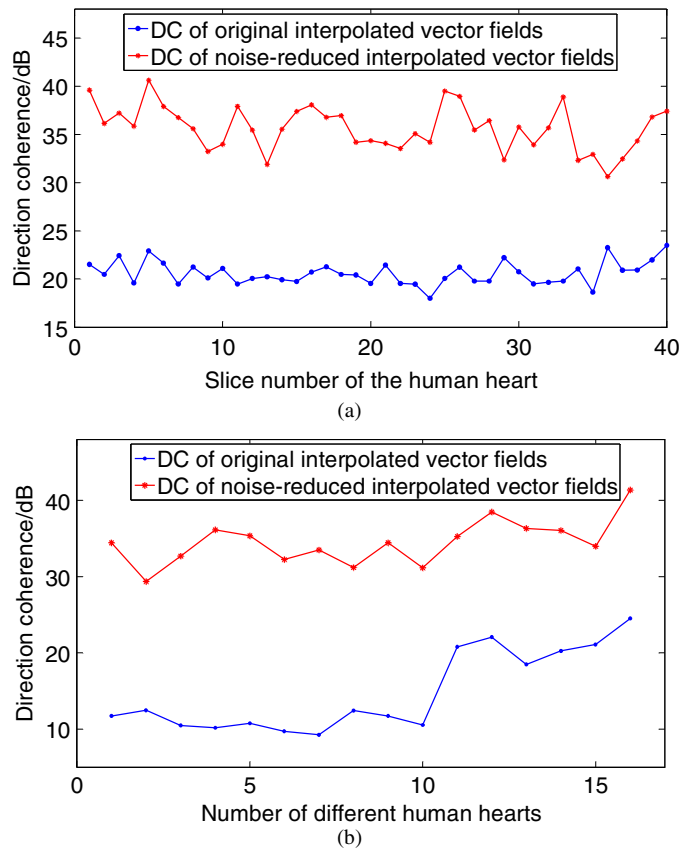


**Figure 5.** DC curves of primary vector fields before and after noise-reduced interpolation. (a) Comparison of DC values before and after interpolation for different slices in the same human heart. (b) Comparison of DC values before and after interpolation for the same slice in different human hearts with different gradient directions.

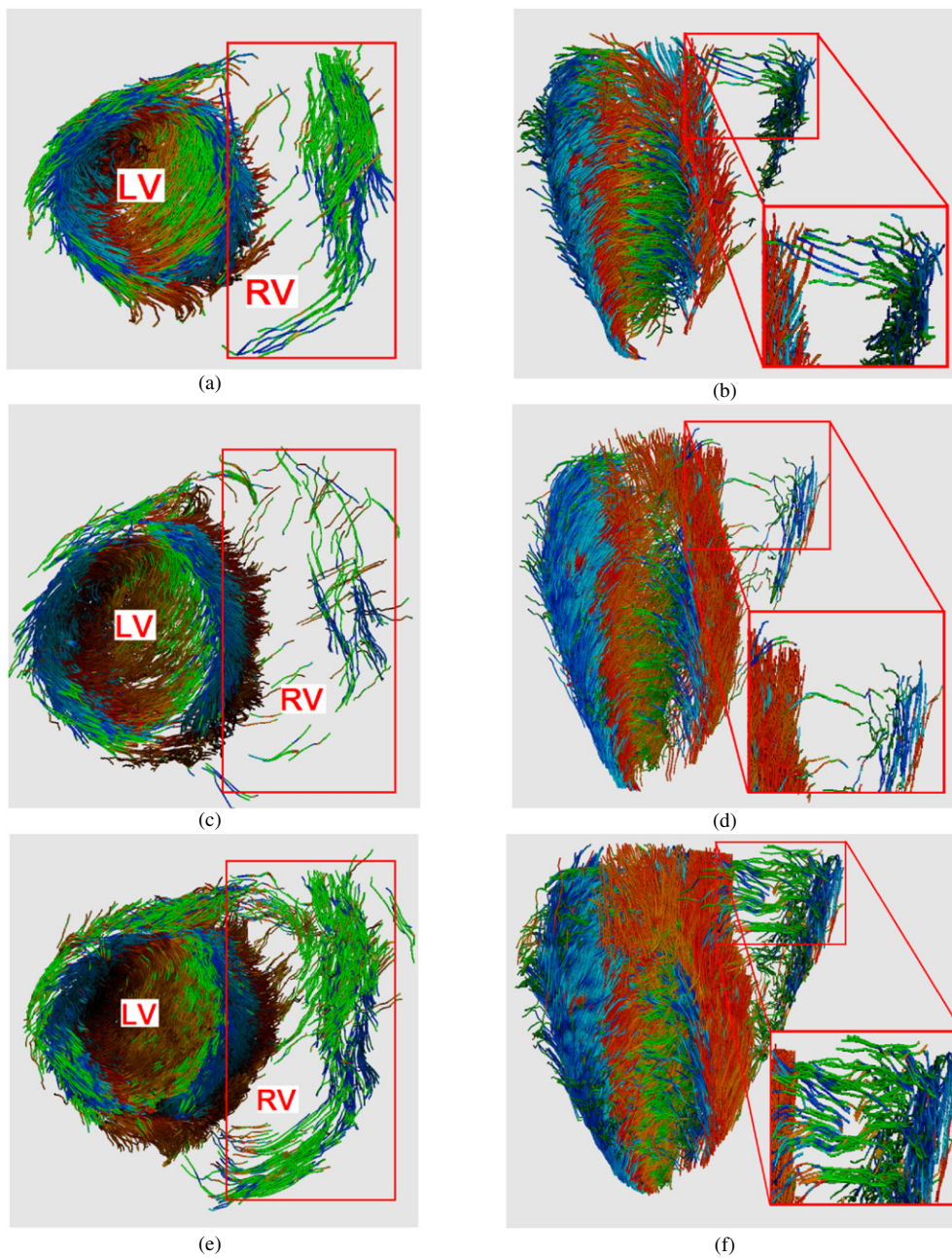
obviously denser after interpolation. However, with the standard bilinear vector interpolation method, the number of noise-corrupted vectors increases. By contrast, with our noise-reduced interpolation, the primary eigenvector field is smoother, and structure details (such as myocardium shape and fiber orientations) are preserved. Since the primary eigenvector's direction corresponds to the fiber orientation at this position, the fiber tracking of the myocardium from the output of our method should be better and more robust than that with standard bilinear interpolation.

Figure 5 shows the comparison of the DC values of vector fields before and after noise-reduced interpolation for two different slices in the same human heart and for the same slice but in different human hearts. The results show that the proposed method improves the DC of primary vector fields by increasing its values by about 15 dB in average, compared to the results obtained by direct interpolation of the original vector fields. In other words, vectors are more coherent after our noise-reduced interpolation. Note that the DC curve varies irregularly; this is caused by the fact that the shape of the myocardium, especially in the right ventricle, is rather irregular and varies greatly from the slice near the base to the

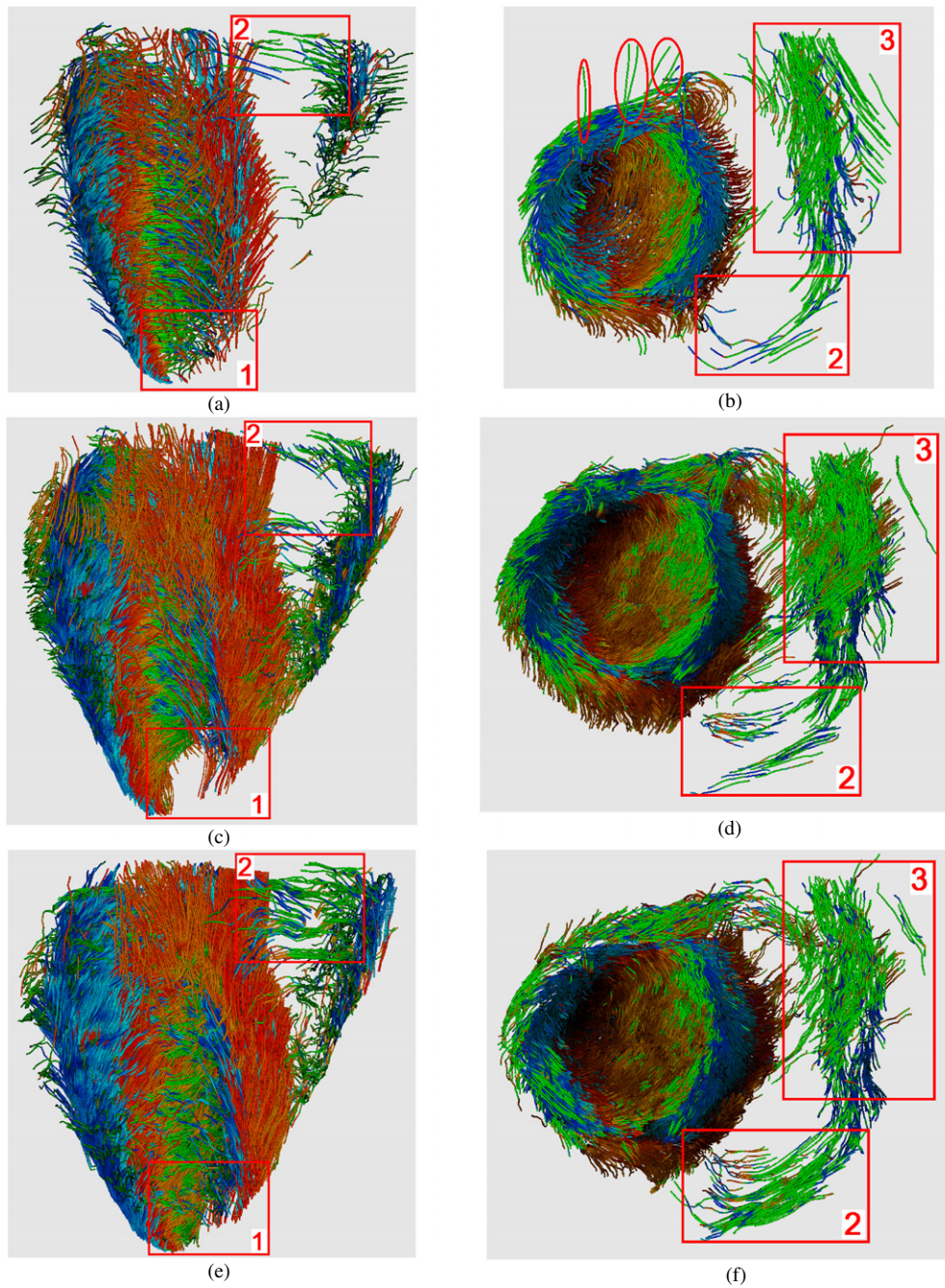
slice near the apex. Figure 5(a) shows that DC values from slice 10 to slice 20 are rather close (blue line). This is due to the fact that the myocardium shapes of the corresponding slices are similar. After the noise-reduced interpolation, the slices do not have the same DC increasing. For example, the DC of the 13th slice is close to that of its neighboring slices before denoising, whereas after denoising, it becomes smaller than those of its neighboring slices, which implies that the vector field corresponding to the 13th slice is the most coherent, compared to its neighboring slices. The more coherent the vector field (or equivalently, the smaller the number of noise-corrupted vectors), the smaller the difference between the denoised and original vector fields (i.e. the smaller the increase of DC). Figure 5(b) displays the DC variations before and after interpolation for the 16 hearts acquired under clinical conditions. Our proposed method always produces greater DC values regardless of the number of gradient directions.

Figure 6 provides an example of fiber tracking improvement when using the proposed noise-reduced interpolation for primary vector fields. It concerns a human heart dataset with 52 slices; the conventional streamline algorithm is used to track the fibers. The visualization uses a color-coded representation of the eigenvector's directions. The left column of figure 6 shows top views of the fiber architecture, while the right column displays lateral views. We observe that the fibers are sometimes discontinuous (or even disappear) in some parts of the right ventricle, because the primary eigenvectors in these regions are so incoherent or so sparse that it is impossible or difficult to track fibers using the streamline algorithm. Comparing the normal and sparse regions in figure 6(a) to those in figure 6(c) (those regions correspond to the left and right ventricles, respectively), we observe that the fibers obtained from standard bilinear interpolation become denser in the normal region, but no possible effect is produced in the sparse region. In fact, the fibers in the sparse region become sparser and more disordered, as can be seen in the boxed region in figures 6(c) and (d). This is because the number of noise-corrupted eigenvectors in the sparse regions increases and the interpolated vector field becomes even more incoherent after interpolation. As a result, fibers are more difficult to be formed and altered by the noise-corrupted vectors. In the case of the vector field processed with our method, the fibers in both the normal and sparse regions become significantly denser and smoother (see figures 6(e) and (f)). The reason is that the corresponding primary eigenvectors are more coherent after our noise-reduced interpolation, which makes the fiber easier to be tracked when using the streamline algorithm.

Figures 7(a) and (b) show the results of fiber tracking obtained from original tensor fields, (c) and (d) the results obtained after using the tensor field interpolation, and (e) and (f) the results after using the noise-reduced vector field interpolation. We observe consistent spiral fiber architecture with the three approaches. It follows that interpolation or denoising can be carried out at the level of the vector field, at least for fiber tracking. Note that the fibers in region 1 become more discontinuous after interpolating the original tensor fields. This is because the original tensor fields are disordered in region 1, and this disorder is amplified by interpolation. By contrast, using our noise-reduced vector field interpolation, the computed fibers in region 1 are smoother and denser. The same effect can be observed in region 2. In region 3, the fibers obtained after using tensor field interpolation seem denser than those obtained after using the noise-reduced vector field interpolation. This indicates that for the normal region (non-sparse region), fiber tracking from the interpolated tensor fields can produce better results than those from the interpolated vector fields (figure 7). However, in some situations, it is not always possible to obtain tensor information. This is, for example, the case when using the polarized light microscope to study fiber architecture (Jouk *et al* 2000). In all cases, the fibers obtained from either vector field interpolation or tensor field interpolation are much denser than those obtained from original tensor fields. The fibers marked by the three red circles in the results



**Figure 6.** Fiber tracking from the primary vector fields in human cardiac DT-MRI. Red rectangles marked with LV and RV indicate the normal and sparse regions of the right ventricle, respectively; (a) and (b) fiber tracking from original vector fields; (c) and (d) fiber tracking from bilinear vector interpolation; (e) and (f) fiber tracking from noise-reduced and interpolated vector fields.



**Figure 7.** Results of fiber tracking using vector field interpolation and tensor field interpolation; (a) and (b) fiber tracking from DW images without interpolation; (c) and (d) fiber tracking using tensor field interpolation in Log-Euclidean space; (e) and (f) fiber tracking using the proposed noise-reduced vector field interpolation.

of fiber tracking from the original tensor fields (figure 7(b)) are artifacts: they are disordered and outside the helix of the left ventricle.

#### 4. Conclusion

We have presented a new method for simultaneously interpolating and denoising human cardiac primary vector fields. By first localizing the noise-corrupted vectors using local information, then restoring them using local TPS interpolation, and finally applying global TPS interpolation, the method allows us to achieve higher resolution, while preserving details and obtaining better direction coherence (DC). The results demonstrate that the proposed method improves the DC by about 15 dB in average and the visual quality of the elevation and azimuth angle maps, and yields smoother and denser fiber tracking for the myocardium. This makes it an interesting tool for the analysis of multicenter studies of the human hearts and the comparative study of myocardial fiber structures coming from DT-MRI and a polarized light microscope. Although developed for cardiac DT-MRI, the proposed method can be readily applied to DT-MRI data of other organs such as the brain.

#### Acknowledgments

This work was partly supported by the joint project of French ANR 2009 (under ANR-09-BLAN-0372-01) and Chinese NSFC (under 30911130364), High Technology Research Development Plan (863 plan) of People's Republic of China (under 2006AA020805), the NSFC of China (under 30670574), Shanghai International Cooperation Grant (under 06SR07109), the INSA Lyon (under BQR 2008/2009) and Region Rhône-Alpes of France (under the project Mira Recherche 2008).

#### References

- Arsigny V, Fillard P, Pennec X and Ayache N 2005 Fast and simple computations on tensors with log-Euclidean metrics *Research Report 5584* INRIA
- Arsigny V, Fillard P, Pennec X and Ayache N 2006 Log-Euclidean metrics for fast and simple calculus on diffusion tensors *Magn. Reson. Med.* **56** 411–21
- Astola J, Haavisto P and Neuvo Y 1990 Vector median filters *Proc. IEEE* **78** 678–89
- Basser P J, Mattiello J and Le Bihan D 1994a MR diffusion tensor spectroscopy and imaging *Biophys. J.* **66** 259–67
- Basser P J, Mattiello J and Le Bihan D 1994b Estimation of the effective self-diffusion tensor from the NMR spin echo *J. Magn. Reson. B* **103** 247–54
- Basser P J and Pajevic S 2000 Statistical artifacts in diffusion tensor MRI (DTMRI) caused by background noise *Magn. Reson. Med.* **44** 41–50
- Principal Warps Bookstein F L 1989 Thin-plate splines and decomposition of deformations *IEEE Trans. Pattern Anal. Mach. Intell.* **11** 567–85
- Cathier P and Ayache N 2004 Isotropic energies, filters and splines for vector field regularization *J. Math. Imaging Vis.* **20** 251–65
- Coulon O, Alexander D C and Arridge S R 2004 Diffusion tensor magnetic resonance image regularisation *Med. Image Anal.* **8** 47–67
- Davis M H, Khotanzand A, Flaming D P and Harms S E 1997 A physics-based coordinate transformation for 3-D image matching *IEEE Trans. Med. Imaging* **16** 317–28
- Duchon J 1977 Splines minimizing rotation invariant seminorms in Sobolev spaces *Constructive Theory of Functions of Several Variables* vol 571 (Berlin: Springer) pp 85–100
- Holmes A, Scollan D and Winslow R L 2000 Direct histological validation of diffusion tensor MRI in formaldehyde-fixed myocardium *Magn. Reson. Med.* **44** 157–61
- Jouk P S, Usson Y, Michalowicz G and Grossi L 2000 Three-dimensional cartography of the pattern of the myofibres in the second trimester fetal human heart *Anat. Embryol.* **202** 103–18

- Kim K H, Ronne I, Formisano E, Goebel R, Ugurbil K and Kim D S 2004 Robust fiber tracking method by vector selection criterion in diffusion tensor images *Conf. Proc. IEEE Engineering in Medicine and Biology Society* pp 1080–3
- Sprengel R, Rohr K and Stiehl H S 1996 Thin-plate spline approximation for image registration *Engineering in Medicine and Biology Society, Bridging Disciplines for Biomedicine. Proc. 18th Annu. Int. Conf. of the IEEE* pp 1190–1
- Trahanias P, Karakos D and Venetsanopoulos A 1996 Directional processing of color images: theory and experimental results *IEEE Trans. Image Process.* **5** 868–81
- Tschumperlé D and Deriche R 2003 Vector-valued image regularization with PDE's: a common framework for different applications *IEEE Conf. on Computer Vision and Pattern Recognition* pp 651–6
- Viero T, Oistamo K and Neuvo Y 1994 Three-dimensional median-related filters for color image sequence filtering *IEEE Trans. Circuits Syst. Video Technol.* **15** 129–42
- Westenberg M A and Ertl T 2004 Vector wavelet thresholding for vector field denoising *IEEE Visualization 2004 Posters Compendium* pp 123–4
- Westenberg M A and Ertl T 2005 Denoising 2-D vector fields by vector wavelet thresholding *J. WSCG* **13** 33–40
- Xia X G and Suter B W 1996 Vector-valued wavelets and vector filter banks *IEEE Trans. Signal Process.* **44** 508–18
- Yang F, Song X, Rapacchi S, Fanton L, Croisille P and Zhu Y M 2009 Noise-reduced TPS interpolation of primary vector fields for fiber tracking in human cardiac DT-MRI *FIMH '09 LNCS* 5528 pp 78–86
- Yoruk E and Acar B 2005 Structure preserving regularization of DT-MRI vector fields by nonlinear anisotropic diffusion filtering *Proc. of European Signal Processing Conference (EUSIPCO) (Antalya, Turkey)*
- Zhao X, Wang M S, Gao W and Liu H Y 2005 White matter fiber tracking method by vector interpolation with diffusion tensor imaging data in human brain *IEEE Engineering in Medicine and Biology Society (China)* pp 5786–9